

Stokes/anti-Stokes Raman spectroscopy of $Al_{0.86}Ga_{0.14}N$ semiconductor alloy

Yuru Lin(林玉茹), Yu Li(李宇), Binbin Wu(吴彬彬), Jingyi Liu(刘静仪), Ruiang Guo(郭睿昂), Yangbin Wang(王扬斌), Qiwei Hu(胡启威), and Li Lei(雷力)

Citation: Chin. Phys. B, 2025, 34 (**5**): 057802. DOI: 10.1088/1674-1056/adb67d
http://cpb.iphy.ac.cn; http://iopscience.iop.org/cpb

What follows is a list of articles you may be interested in

Development of small pixel HgCdTe infrared detectors

Ming Liu(刘铭), Cong Wang(王丛), Li-Qing Zhou(周立庆)
Chin. Phys. B, 2019, 28 (**3**): 037804. DOI: 10.1088/1674-1056/28/3/037804

Roles of voltage in semi-insulating GaAs photoconductive semiconductor switch

Hai-Juan Cui(崔海娟), Hong-Chun Yang(杨宏春), Jun Xu(徐军), Yu-Ming Yang(杨宇明), Zi-Xian Yang(杨子贤)
Chin. Phys. B, 2017, 26 (**1**): 017804. DOI: 10.1088/1674-1056/26/1/017804

Effect of pressure on the semipolar GaN (10-11) growth mode on patterned Si substrates

Liu Jian-Ming (刘建明), Zhang Jie (张洁), Lin Wen-Yu (林文禹), Ye Meng-Xin (叶孟欣), Feng Xiang-Xu (冯向旭), Zhang Dong-Yan (张东炎), Steve Ding, Xu Chen-Ke (徐宸科), Liu Bao-Lin (刘宝林)
Chin. Phys. B, 2015, 24 (**5**): 057801. DOI: 10.1088/1674-1056/24/5/057801

Mid-gap photoluminescence and magnetic properties of GaMnN films grown by metal-organic chemical vapor deposition

Xing Hai-Ying (邢海英), Xu Zhang-Cheng (徐章程), Cui Ming-Qi (崔明启), Xie Yu-Xin (谢玉芯), Zhang Guo-Yi (张国义)
Chin. Phys. B, 2014, 23 (**10**): 107803. DOI: 10.1088/1674-1056/23/10/107803

N vacancy, substitutional O, and Al defects in the bandgap of composition-tunable nonstoichiometric AlN powder

Zhang Dian (张电), Liu Fa-Min (刘发民), Cai Lu-Gang (蔡鲁刚)
Chin. Phys. B, 2014, 23 (**6**): 067803. DOI: 10.1088/1674-1056/23/6/067803

Stokes/anti-Stokes Raman spectroscopy of $Al_{0.86}Ga_{0.14}N$ semiconductor alloy

Yuru Lin(林玉茹)[1], Yu Li(李宇)[1], Binbin Wu(吴彬彬)[1], Jingyi Liu(刘静仪)[1], Ruiang Guo(郭睿昂)[1], Yangbin Wang(王扬斌)[1], Qiwei Hu(胡启威)[2,‡], and Li Lei(雷力)[1,†]

[1] *Institute of Atomic and Molecular Physics, Sichuan University, Chengdu* 610065, *China*

[2] *School of Physics and Electronic Engineering, Sichuan University of Science and Engineering, Zigong* 643000, *China*

(Received 27 November 2024; revised manuscript received 8 February 2025; accepted manuscript online 15 February 2025)

The lattice dynamics of a high Al composition semiconductor alloy, $Al_{0.86}Ga_{0.14}N$, in comparison with intrinsic GaN and AlN are studied by Stokes/anti-Stokes Raman spectroscopy in the temperature range of 85–823 K. The phonon anharmonic effect in $Al_{0.86}Ga_{0.14}N$ is found to be stronger than that in GaN, revealing low thermal conductivity in the semiconductor alloy. Multi-phonon coupling behavior is analyzed by both Stokes Raman and anti-Stokes Raman spectroscopy. It is interesting to find that the anti-Stokes scattering exhibits stronger three-phonon coupling than the Stokes scattering, which may be due to the fact that the anti-stokes scattering process is generated from an excited state and the scattered photons have higher energies. The Stokes/anti-Stokes temperature correction factor β for Raman modes in $Al_{0.86}Ga_{0.14}N$ alloy are all smaller than those of the corresponding intrinsic modes in GaN and AlN. The reasons for the difference in β can be attributed to three aspects, including the equipment setups, materials properties (the binding energy) and the coupling strength of Raman scattering and the sample.

Keywords: $Al_xGa_{1-x}N$, semiconductor alloy, Stokes/anti-Stokes Raman spectroscopy, two-mode behavior, multi-phonon coupling

PACS: 78.30.Fs, 74.25.nd, 33.20.Fb, 63.20.kg

DOI: 10.1088/1674-1056/adb67d **CSTR:** 32038.14.CPB.adb67d

1. Introduction

GaN and AlN are important wide-bandwidth semiconductor materials, and their direct bandgap energies are about 3.4 eV and 6.2 eV, respectively.[1] They have the advantages of high temperature resistance, high melting point, low thermal conductivity and high breakdown electric field, and are widely used in blue and violet light emission devices.[2,3] $Al_xGa_{1-x}N$ semiconductor alloy (formed by Al atoms replacing some of the Ga atoms) can achieve continuous tuning of the band gap from 3.4 eV to 6.2 eV. Therefore, the band gap can be adjusted by making different alloying substances with different content x.[4] Because of this feature, it has broad application prospects in blue, green, ultraviolet and white light-emitting diodes.[5] There has been great interest in the fundamental properties of such materials.[6–8] Although significant progress has been made in the preparation of such materials in recent years, synthesizing semiconductor alloys with high Al content is relatively difficult as compared to those with low Al content. As the aluminum content increases, the doping efficiency of $Al_xGa_{1-x}N$ decreases, making it difficult to synthesize high aluminum content $Al_xGa_{1-x}N$ alloys. Therefore, our understanding of the lattice dynamics of this alloy sample is still limited. Secondly, the low thermal conductivity of $Al_xGa_{1-x}N$ alloys results in a short lifespan of the device in practical applications. The presence of thermal phonons inside the alloy can affect the relaxation process of charge carriers, thereby reducing the performance and saturation drift velocity of the device.[9] Therefore, understanding the physical mechanism of the low thermal conductivity of the alloy will be conducive to the further development of its devices.

Vibration spectroscopy, such as Raman spectroscopy, could reveal information on the stress state, phonon coupling and defects of alloy materials. The experimental data of the temperature-dependent Raman line width and Raman shift can also be compared with the predictions of the anharmonic crystal theory.[10–12] The lattice dynamics of hexagonal $Al_xGa_{1-x}N$ alloys have been studied theoretically and experimentally in many publications.[13–15] In $Al_xGa_{1-x}N$ alloys, the two vibrational modes, A_1(LO) and E_1(LO), exhibit a typical "one-mode" behavior. This behavior refers to the approximately linear variation trend of the frequency of each Raman mode with the change of x in the alloy. However, due to mixing and crossing effects, three vibrational modes, A_1(TO), E_1(TO) and E_2^{high}, instead exhibit "two-mode" behavior in $Al_xGa_{1-x}N$ alloys with high-Al compositions ($x > 0.6$). The phonon frequencies of the two sets of vibrational modes show an approximately linear trend from $x = 0$ and $x = 1$ with the doping composition x.[4] The work of Davydov *et al*.

†Corresponding author. E-mail: lei@scu.edu.cn

‡Corresponding author. E-mail: hqw920861@163.com

© 2025 Chinese Physical Society and IOP Publishing Ltd. All rights, including for text and data mining, AI training, and similar technologies, are reserved.

describes the first- and second-order Raman spectroscopy of $Al_xGa_{1-x}N$ alloys over the entire composition range, tracing in detail the frequency of all active phonon modes in Raman scattering as a function of composition, and well illustrates the "two-mode" behavior of the Raman phonons of $Al_xGa_{1-x}N$ alloys with high-Al compositions.[16] Meanwhile, some scholars have investigated the temperature-dependent Raman shift of $Al_xGa_{1-x}N$ semiconductor alloys with different compositions using two materials, an AlGaN/GaN stack[17] and AlGaN/GaN heterostructures.[18,19] Pomeroy *et al.* used anti-Stokes Raman scattering spectroscopy and conventional Raman thermography techniques to detect thermal phonons in the channels of active AlGaN/GaN high electron mobility transistors (HFETs).[9] At present, studies on the Stokes and anti-Stokes Raman spectra of high-Al compositions of $Al_xGa_{1-x}N$ alloys remain scarce. Moreover, the relationship between the "two-mode" behavior of $Al_xGa_{1-x}N$ alloys and the vibration mode of the intrinsic sample is still an open question. By studying the phonon anharmonic effect of materials, the reasons for low thermal conductivity could also be revealed, which has profound guiding significance for the application of their devices. There are almost no lattice dynamics studies of $Al_xGa_{1-x}N$ alloys on the basis of anti-Stokes Raman spectroscopy. By using both Stokes and anti-Stokes Raman spectroscopy, the results of multi-phonon coupling could be further revealed, and the correction factor (β) that strongly correlates with *in situ* Stokes/anti-Stokes temperature measurement could also be obtained.

In this paper, temperature-dependent Stokes/anti-Stokes Raman spectroscopy experiments were carried out in the temperature range of 85 K to 823 K on a high-Al composition $Al_{0.86}Ga_{0.14}N$ single crystal, in comparison with its intrinsic AlN microcrystal and GaN single crystal. The lattice dynamics behaviors were investigated on the basis of the obtained Stokes/anti-Stokes Raman spectroscopy and the temperature correction factor β has also been analyzed.

2. Experimental procedure

In this work, a single crystal sample of $Al_{0.86}Ga_{0.14}N$ approximately 1 mm in size was used for the Raman experiments. For comparison, a single crystal GaN sample ($\sim$ 1 cm in size) and high-purity microcrystal AlN samples with grain size of 2 μm were selected. The structural and chemical properties of the studied samples have been reported in our previous work.[20] According to the characterization results, there is no potential phase separation phenomenon in the crystallinity of the materials.

The Stokes/anti-Stokes Raman experiment was carried out in the Extreme-condition Science Laboratory (ESL) at Sichuan University.[21,22] The Raman spectra were acquired

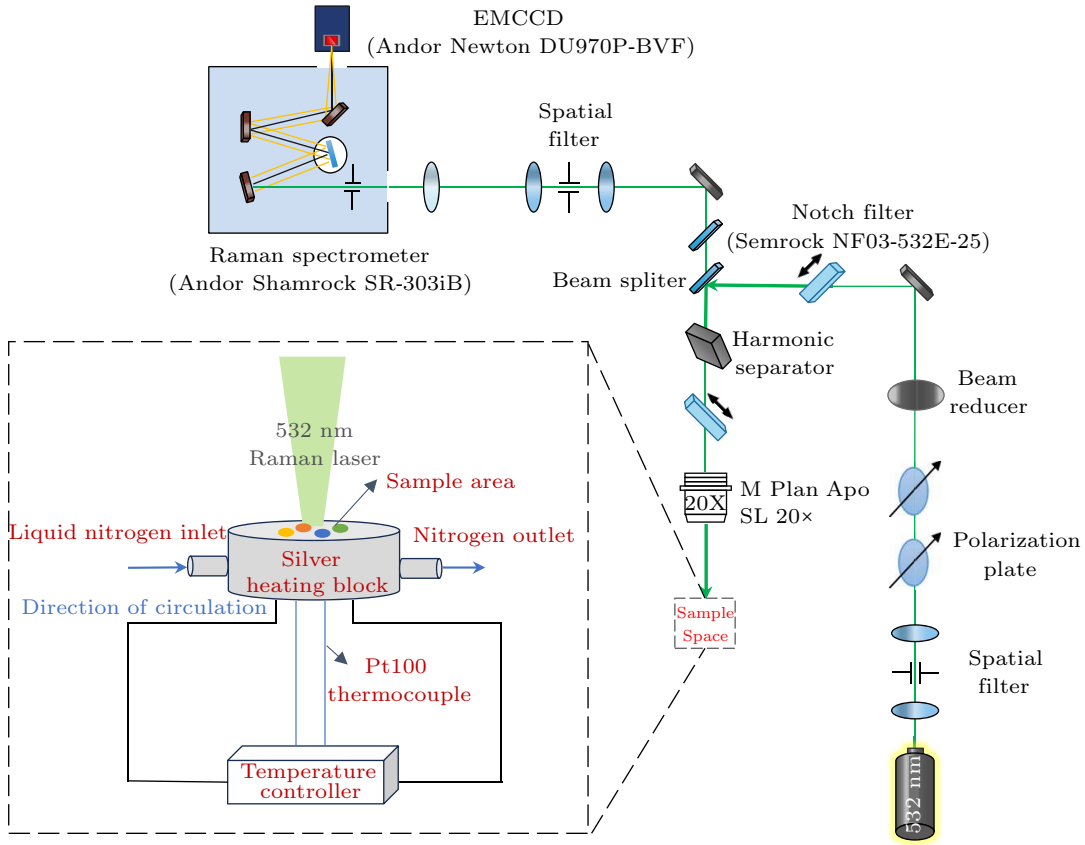


Fig. 1. The optical system layout in this study. The box shows a sketch of the hot/cold stage.

with a 532 nm solid-state laser (RGB Nova Pro, 300 mW) with a laser spot size of about 5 μm. The objective lens employed in this work was a Mitutoyo M Plan Apo SL 20× (W.D. = 34 mm, N.A. = 0.28), and the backscattered light was passed through an achromatic objective and a notch filter (Semrock NF03-532E-25). It was collected by a Raman spectrometer (Andor Shamrock SR-303i-B) with an 1800 g·mm^{-1} holographic grating resolution of 0.5 cm^{-1} and an EMCCD (Andor Newton DU970P-BVF). To collect the spectral data, the typical exposure time was 3 s, the accumulation number was 20 times and the laser output power as 40 mW. However, the laser power on the sample was less than 2.33 mW. Before the Raman experiment, monocrystalline silicon (520 cm^{-1}) was used for system calibration. Figure 1 shows the optical path diagram used in this work.

The hot/cold stage (THMS600, Linkam) was used for the temperature-dependent Raman experiments in the range from 85 K to 823 K. A silver heating block with high thermal conductivity was used to heat the sample, while liquid nitrogen was utilized for the cooling process. The temperature of the sample was measured by the thermal effect of a thermocouple (Pt100 type) with an accuracy of no more than ±1 K. The Stokes/anti-Stokes Raman spectra were collected in the range of 300 K to 823 K with the step size of 50 K.

In this work, spectral analysis software Peakfit4.12 was used for data fitting. The program allows peak fitting using a combination of Lorentzian and Gaussian functions as well as deductions from the background. Both the anti-Stokes and Stokes Raman lines were fitted by the Voigt or Lorentzian functions after noise removal.

3. Results and discussion

3.1. Group theoretical analysis for the Raman active modes

According to literature reports, hexagonal AlN and GaN have a wurtzite-type structure with space group $P6_3mc$ (C_{6v}^4), while the group theory analysis shows that there are six optical phonon modes: $\Gamma_{\text{opt}} = \text{A}_1 + 2\text{B} + \text{E}_1 + 2\text{E}_2$, of which A_1, E_1 and E_2 are Raman-active modes, and the B mode is a quiet mode. Because of the LO–TO splitting of the A_1 and E_1 vibrational modes, there are six Raman-active vibrational modes in the center of the Brillouin zone, which can be expressed as

$$\begin{aligned}\Gamma_{\text{Raman}} = {} & \text{A}_1(\text{TO}) + \text{A}_1(\text{LO}) + \text{E}_1(\text{TO}) \\ & + \text{E}_1(\text{LO}) + \text{E}_2^{\text{low}} + \text{E}_2^{\text{high}}.\end{aligned}$$

Figure 2 shows that the Raman peak splitting fits for AlN, GaN and $\text{Al}_{0.86}\text{Ga}_{0.14}\text{N}$ samples at room temperature. There are a number of extensive studies in the literature on the Raman vibrational modes of AlN and GaN samples with hexagonal lattice structures.[10,23,24] As shown in Figs. 2(a) and 2(b), AlN and GaN have five Raman modes, which are different from the number of Raman modes reported in the previous literature and exhibit an absence of E_2^{low} vibration modes. This is because a trap filter is used to suppress Rayleigh scattering, which attenuates up to 250 cm^{-1}, making it impossible to measure the low-frequency E_2^{low} vibration mode. Figure 2(c) clearly shows the two-mode behavior of $\text{Al}_{0.86}\text{Ga}_{0.14}\text{N}$ samples. The frequencies of the nine peaks are 588.3 cm^{-1}, 600.5 cm^{-1}, 615.7 cm^{-1}, 625.1 cm^{-1}, 638.3 cm^{-1}, 658.5 cm^{-1}, 664.1 cm^{-1}, 890.0 cm^{-1} and 899.1 cm^{-1}. According to the equation of Al content and $\text{Al}_x\text{Ga}_{1-x}\text{N}$ Raman peak position reported in the literature,

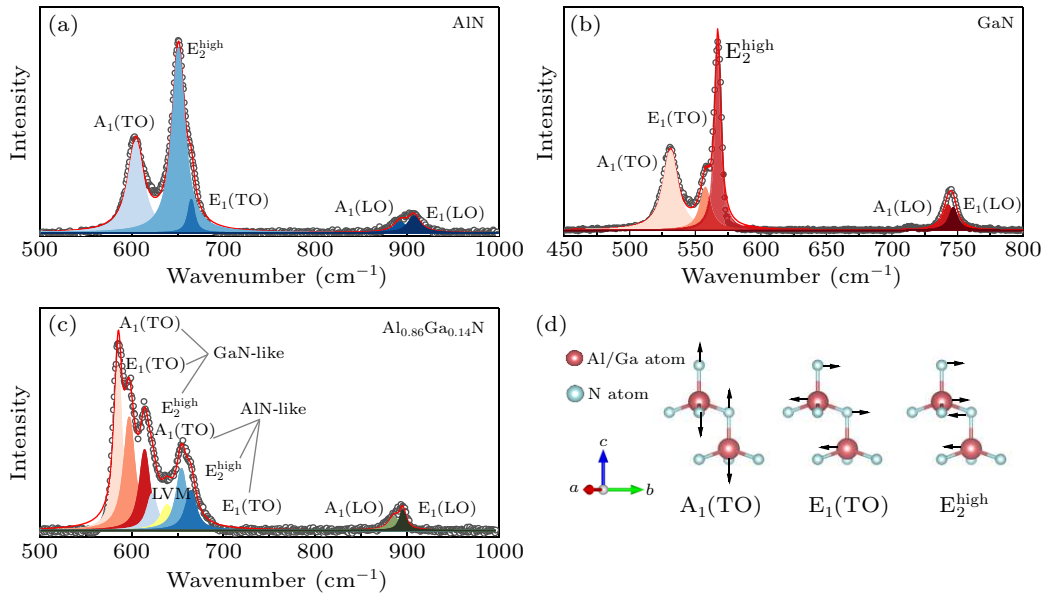


Fig. 2. Lorentzian-fitted Raman spectra of (a) AlN and (b) GaN, and Voigt-fitted Raman spectrum of (c) $\text{Al}_{0.86}\text{Ga}_{0.14}\text{N}$ at room temperature; (d) the atomic displacement of different Raman modes for hexagonal wurtzite-type AlN (GaN).[25]

the Al content of $Al_xGa_{1-x}N$ alloy is 0.86, which is the same as the EDS result.[16,20]

3.2. Stokes and anti-Stokes Raman scattering

Figure 3 shows the temperature-dependent Stokes and anti-Stokes Raman scattering for AlN, GaN and $Al_{0.86}Ga_{0.14}N$ with 532 nm laser excitation. As can be seen from Fig. 3, the intensity of the Stokes Raman peaks for AlN and GaN samples decreased with the increase of temperature, while the intensity of the anti-Stokes peak increased. The intensities of Raman peaks for $Al_{0.86}Ga_{0.14}N$ material are the same as those of the two intrinsic materials, AlN and GaN. By fitting the Raman frequency of the sample, it is found that the Raman modes have similar temperature dependence. With the increase of temperature, all Raman modes move to the low frequency direction.

In this work, we focus on the lattice dynamics of three Raman modes exhibiting a "two-mode" behavior in the $Al_{0.86}Ga_{0.14}N$ sample. The temperature dependence of the phonon frequency and damping originates from the anharmonic term in the lattice vibration Hamiltonian.[26] The temperature-dependent Raman shift can be expressed as the result of two additive effects, one is the frequency change caused by thermal expansion or volume change and the other is the anharmonic coupling with phonons from other branches.[27] The Raman shifts of these modes can be well represented as a quadratic equation: $\omega = \omega_0 - \alpha_1 T - \alpha_2 T^2$, where ω_0 is the Raman frequency shift obtained when the temperature $T = 0$ K, α_1 and α_2 represent the first- and second-order temperature coefficients, respectively, and the data fitting of the scatter plot of the Raman shift with temperature-dependent is carried out through the function. The values of the fitting parameters are shown in Table 1.

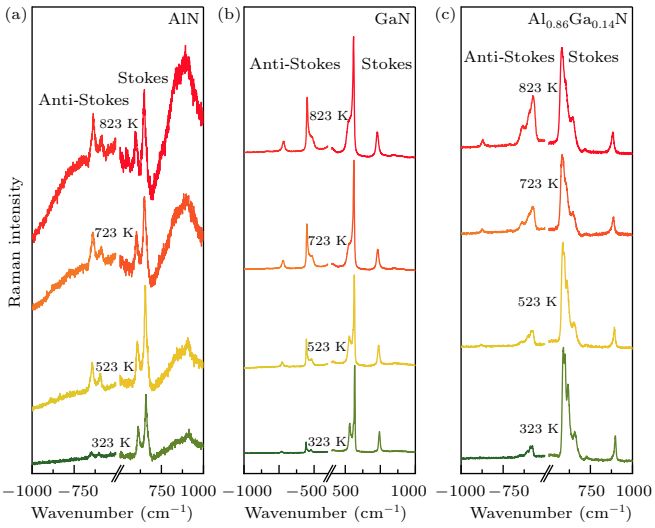


Fig. 3. Typical high-temperature Raman spectra of (a) AlN, (b) GaN and (c) $Al_{0.86}Ga_{0.14}N$. The Raman displacement measurements shown in the figure range from -1000 cm^{-1} to 1000 cm^{-1}, with Stokes and anti-Stokes Raman spectra selected for four typical temperature points.

Table 1. The parameters of the quadratic function fitting results of Raman spectra for AlN, GaN and $Al_{0.86}Ga_{0.14}N$ alloy. GaN-like and AlN-like modes are the GaN-like modes and AlN-like modes in $Al_{0.86}Ga_{0.14}N$ alloy, respectively.

Mode	Sample	ω_0 (cm^{-1})	α_1 (10^{-3} cm^{-1}·K)	α_2 (10^{-6} cm^{-1}·K^2)
A_1(TO)	GaN	533.4	0.9	9.7
	GaN-like	593.1	11.3	18.8
	AlN	618.8	9.2	18.9
	AlN-like	630.2	23.3	−4.2
E_1(TO)	GaN	560.2	4.9	11.0
	GaN-like	605.1	12.3	10.6
	AlN	675.8	9.9	8.4
	AlN-like	674.0	60.3	−28.3
E_2^{high}	GaN	570.0	4.7	9.8
	GaN-like	622.8	26.2	−2.4
	AlN	662.6	10.7	9.2
	AlN-like	677.2	39.3	−9.7

The temperature-dependent Raman shift can be expressed as the result of two effects, one is the change due to the thermal-expansion effect and the other is due to phonon anharmonic effects. Raman shift can be expressed as a function of temperature, written as $\Omega(T) = \Omega_0 + \Omega^{(1)}(T) + \Omega^{(2)}(T)$. Ω_0 represents the optical mode of the harmonic frequency, $\Omega^{(1)}(T)$ is a thermal expansion of the contribution of Raman shift and $\Omega^{(2)}(T)$ is the phonon anharmonic coupling.

$$\Omega^{(1)}(T) = \Omega_0 \left\{ \exp\left[-3\gamma \int_0^T \alpha(T') \mathrm{d}T' \right] - 1 \right\}, \quad (1)$$

where γ is the Gruneisen parameter for the optical Raman mode. $\alpha(T')$ represents the material linear thermal expansion coefficient, which is related to the temperature. The linear thermal expansion coefficients of GaN[28] and AlN[2] have been reported in literature. The linear thermal expansion coefficient of $Al_{0.86}Ga_{0.14}N$ was calculated in Refs. [2,28]. The anharmonic coupling terms are caused by the third, fourth and higher order anharmonic terms in the Hamiltonian and can be modeled as

$$\Omega^{(2)}(T) = A\left\{1 + \sum_{i=1}^{2} \frac{1}{(\mathrm{e}^{x_i} - 1)}\right\} + B\left\{1 + \sum_{j=1}^{3}\left[\frac{1}{(\mathrm{e}^{y_j} - 1)} + \frac{1}{(\mathrm{e}^{y_i} - 1)^2}\right]\right\}, \quad (2)$$

where A and B are the fitting parameters for the three-phonon process and the four-phonon process, respectively, and $x_1 + x_2 = y_1 + y_2 + y_3 = \hbar\nu_0/k_B T$. The first term of the polynomial is caused by the decay of the zone-center phonon into two phonons (three-phonon process), while the second term represents the decay into three phonons (four-phonon process). The anharmonic phonon–phonon interaction introduces a higher-order term into the Hamiltonian, coupling the harmonic eigenstates and producing finite phonon lifetimes. These peaks are observable in the measured Raman shift and linewidth in the

Raman spectra. Therefore, the analysis of the temperature dependence of Raman spectra can yield valuable information about anharmonic processes.[29] Figure 4 briefly illustrates the three-phonon and four-phonon processes.

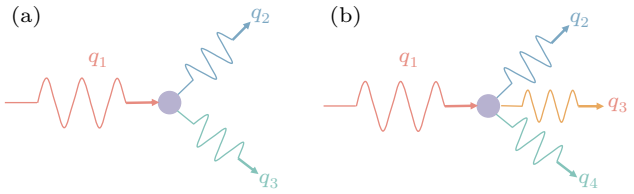


Fig. 4. Schematic diagrams of (a) the three-phonon process and (b) the four-phonon process.

Combining all the above formulas, the modeling formula of temperature by Raman frequency shift can be expressed as[27]

$$\Omega(T) = \Omega_0 \exp\left[-3\gamma \int_0^T \alpha(T')\mathrm{d}T'\right] + A\left\{1 + \sum_{i=1}^{2} \frac{1}{(\mathrm{e}^{x_i} - 1)}\right\} + B\left\{1 + \sum_{j=1}^{3}\left[\frac{1}{(\mathrm{e}^{y_i} - 1)} + \frac{1}{(\mathrm{e}^{y_i} - 1)^2}\right]\right\}, \quad (3)$$

where Ω_0 can be obtained by the expression $\omega_0 = \Omega_0 + A + B$. The results of fitting the influence of temperature on Raman shift by using the above formula are shown by the solid line in Fig. 5; notably the fitting results are in good agreement with the experimental data points.

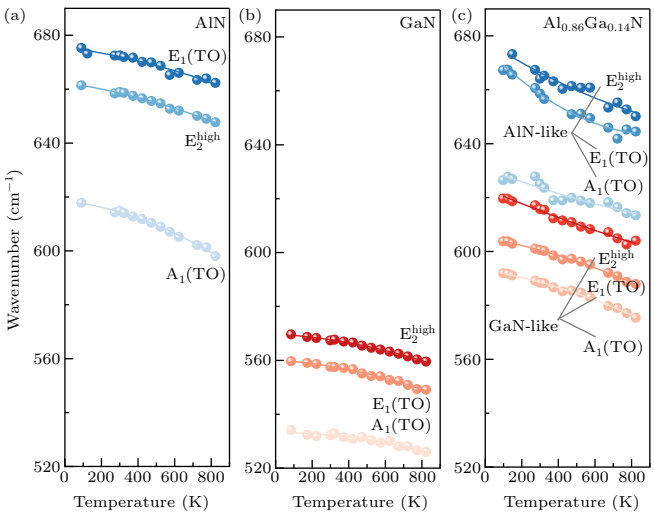


Fig. 5. Raman displacement of each Raman mode in (a) AlN, (b) GaN and (c) $Al_{0.86}Ga_{0.14}N$ at different temperatures. In order to clearly see the response of the vibration mode to temperature for the three samples, a uniform scale is chosen for the horizontal and vertical coordinates of this figure. The solid line in the figure is the result obtained by fitting the experimental data to Eq. (3).

The values of fitting parameters A and B are shown in Table 2. By considering the absolute values of the fitted parameters A and B, it can be seen that the three-phonon coupling process plays a dominant role in the multi-phonon mode at high temperatures for both $Al_{0.86}Ga_{0.14}N$ and its intrinsic materials AlN and GaN. The relative contribution of the three-phonon and four-phonon processes to the total phonon decay can be estimated from the ratio of A/B in Table 2.

Table 2. The parameters of the phonon fitting results of Stokes Raman spectra for AlN, GaN and $Al_{0.86}Ga_{0.14}N$ alloy. γ is the Grüneisen parameters, and A and B are the fitting parameters obtained by fitting Eq. (3).

Mode	Sample	γ	A	B	A/B
A_1(TO)	GaN	1.53	0.352	−0.006	58.7
	GaN-like	1.35	0.016	−0.008	2
	AlN	1.50	0.187	−0.015	12.5
	AlN-like	1.35	0.457	0.005	91.4
E_1(TO)	GaN	1.32	0.185	−0.007	26.4
	GaN-like	1.42	0.016	−0.008	2
	AlN	1.48	0.230	−0.008	28.8
	AlN-like	1.54	−1.094	0.012	91.2
E_2(high)	GaN	1.47	0.284	−0.007	40.6
	GaN-like	1.35	−0.580	0.035	16.6
	AlN	1.66	0.252	−0.009	28
	AlN-like	1.69	−2.010	0.032	62.8

Note: The Grüneisen parameters for GaN,[27] AlN[23] and $Al_{0.86}Ga_{0.14}N$[20] have been reported. The GaN-like and AlN-like modes are the GaN-like modes and AlN-like modes in $Al_{0.86}Ga_{0.14}N$ alloy, respectively.

However, for the $Al_{0.86}Ga_{0.14}N$ sample, the A/B is much smaller than that of GaN, suggesting that the three-phonon process decreases dramatically after Al ion injection, while the chance of the four-phonon process increases.[12] The injection of Al into GaN causes lattice defects and structural disorder, and breaks the translational symmetry of GaN. The temperature dependence of the displacement and linewidth is a direct result of anharmonic effects. As a result of the anharmonic effect, the Raman shift of the intrinsic semiconductor material decreases with increasing temperature. At high temperatures, the interaction between optical phonons increases, leading to enhanced phonon scattering and a shorter phonon lifetime.

In addition, due to the physical principles of the Stokes and anti-Stokes spectroscopy, the differences in multi-phonon fitting results between the two spectra were also taken into account. We selected the Raman mode with the highest peak intensity among three samples, the E_2^{high} mode in GaN and AlN and the A_1(TO) mode in $Al_{0.86}Ga_{0.14}N$, for multi-phonon coupling process analysis. Figure 6 shows the phonon coupling fitting results of GaN, $Al_{0.86}Ga_{0.14}N$ and AlN in the temperature range of 573 K–823 K, with a high degree of agreement between the solid line and the data points.

Meanwhile, the fitting results are shown in Table 3 below. According to the results of the comparison of the absolute values of A and B, no matter what kind of Raman mode is calculated, the three-phonon process is dominant. It is found that the three-phonon coupling is much more significant in the anti-Stokes Raman scattering. This is because the anti-Stokes

Raman scattering is a process in which the phonon is excited to a higher state by the temperature, jumps up to a virtual energy level after absorbing a photon ($h\nu_0$) from the excitation laser, and then jumps back to the ground state and emits a photon with higher energy ($h\nu_2$). Therefore, the anti-Stokes scattering exhibits stronger three-phonon coupling behavior as compared to the Stokes scattering, which may be attributed to the higher excited state phonon and the higher scattering photon energy in the anti-Stokes scattering process. The schematic diagram of this process is illustrated in the Fig. 7 insets.

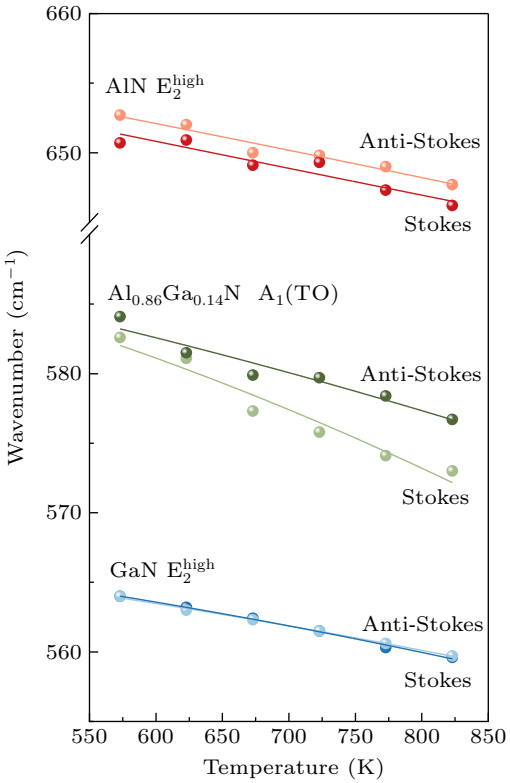


Fig. 6. The temperature dependence of the Stokes and anti-Stokes Raman peaks for three typical modes: GaN E_2^{high}, AlN E_2^{high} and $Al_{0.86}Ga_{0.14}N$ $A_1(TO)$. For comparison, the anti-Stokes Raman wavenumber is shown in the absolute value.

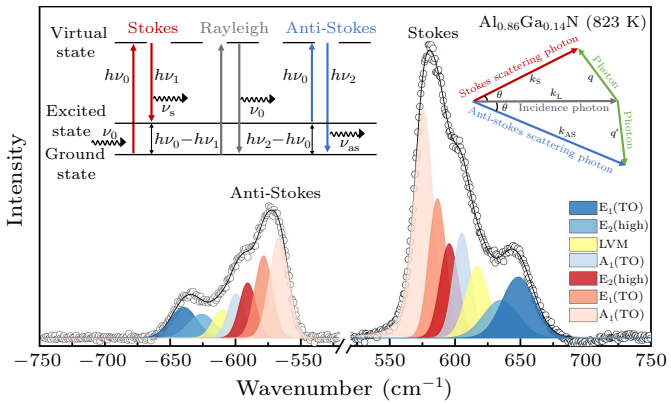


Fig. 7. Stokes and anti-Stokes Raman spectra of $Al_{0.86}Ga_{0.14}N$ alloy at 823 K. The illustration on the left shows a schematic diagram of the energy level transitions for Rayleigh scattering, Stokes scattering and anti-Stokes scattering. The illustration on the right shows the momentum relationship between Stokes and anti-Stokes photon scattering and phonons.

Table 3. The phonon coupling parameters of Stokes and anti-Stokes Raman spectra for AlN, GaN and $Al_{0.86}Ga_{0.14}N$ alloy in 573 K–823 K.

Sample	Mode	Spectrum	A	B	A/B
GaN	E_2^{high}	anti-Stokes	−0.853	0.009	94.78
		Stokes	0.225	−0.006	37.5
$Al_{0.86}Ga_{0.14}N$	A_1(TO)	anti-Stokes	−1.049	0.008	131.13
		Stokes	0.247	−0.017	14.53
AlN	E_2^{high}	anti-Stokes	−1.369	0.020	68.45
		Stokes	0.012	−0.002	6

3.3. Stokes/anti-Stokes thermometric calibration factor

The temperature of the sample can be determined by measuring the intensity ratio of the Stokes and anti-Stokes Raman peaks. The Stokes/anti-Stokes thermometry is based on a detailed balancing principle of the intensity asymmetry of the Stokes and anti-Stokes lines. By measuring the Stokes and anti-Stokes signal intensity of the sample, in combination with the Boltzmann ratio factor, the *in-situ* temperature can be calculated. The relative occupancy of the ground and excited states at thermal equilibrium can be derived from the Boltzmann distribution $\exp(-\frac{hc\nu_i}{kT})$, where T is the absolute temperature and ν_i is the wavenumber of the transition energy between the excited and ground states. As the temperature increases, the intensity of anti-Stokes line increases, while the intensity of Stokes line decreases. This trend increases significantly with the increase of temperature, and is in good agreement with the Boltzmann distribution described in Eq. (4) The high-pressure Raman spectra of liquid H_2 (D_2),[30] the melting line of fluid N_2,[31] the phonon anharmonic effect of hBN[22] and the dynamic barrier of CO_2[32] phase transition have been studied by using this method. Figure 7 shows the Stokes and anti-Stokes Raman spectra of the $Al_{0.86}Ga_{0.14}N$ sample at 823 K. The energy level transition relationships of Rayleigh scattering, Stokes scattering, and anti-Stokes scattering, as well as the momentum relationships in Stokes scattering and anti-Stokes scattering are also shown in the Fig. 7 inset.

$$\frac{I_{AS}}{I_S} = \beta \left(\frac{\nu_0 + \nu_i}{\nu_0 - \nu_i}\right)^4 e^{-\frac{hc\nu_i}{kT}}, \tag{4}$$

where I_{AS}/I_S represents the ratio of the intensity of the anti-Stokes spectral line to that of the Stokes spectral line, ν_0 is the frequency of the excited light source, ν_i is the Raman shift of the sample, h is the Planck constant, c is the speed of light, k is the Boltzmann constant and T is the absolute temperature scale in Kelvin. β is the correction factor, which is considered to be associated with the spectrometer, CCD and other system factors.[33,34] Our previous work further discussed the factor β, which is related to the excitation light source wavelength, the sample Raman shift, the measurement temperature region and other system factors.[22] Therefore, all physical quantities

in Eq. (4) are known except β. The value of β can be calculated on the basis of the principle that the left and right sides of the equation are equal.

The values of the β parameter for the different Raman modes of the three studied samples are shown in Table 4. By analyzing the data in Table 4, it can be found that under the same experimental conditions, the β for each Raman mode of all samples is near 1. Moreover, the β for Raman modes in $Al_{0.86}Ga_{0.14}N$ are smaller than those of the corresponding intrinsic modes in GaN and AlN; and the β for the GaN are smaller than the same Raman mode of AlN. Since the binding energy of GaN is 285 kJ/mol and the binding energy of AlN is 368 kJ/mol, we believe that the difference value in β may be due to the binding energy of the material itself. The β calculated for the material with larger binding energy is larger. In general, we believe that the influencing factors of β can be divided into three aspects, including device parameters, sample properties and Raman scattering coupling with the sample.

Table 4. The correction factor (β) for AlN, GaN and $Al_{0.86}Ga_{0.14}N$ for the Stokes and anti-Stokes spectroscopy. The GaN-like and AlN-like modes are the GaN-like modes and AlN-like modes in $Al_{0.86}Ga_{0.14}N$ alloy, respectively.

Mode	A_1(TO)	E_1(TO)	E_2^{high}
GaN	0.98	0.96	1.06
AlN	1.03	–	1.11
GaN-like	0.82	0.74	0.85
AlN-like	0.84	0.82	0.89

Note: The E_1(TO) Raman mode of AlN cannot obtain fitting intensity data due to the weak anti-Stokes peak intensity, therefore, the β value cannot be calculated.

4. Conclusion

The Stokes/anti-Stokes Raman spectra of $Al_{0.86}Ga_{0.14}N$ in the temperature range of 85 K–823 K were measured and compared with those of intrinsic GaN and AlN. The multi-phonon processes and phonon anharmonic effect were analyzed in detail, and correction factor β and its influencing factors, which are strongly correlated with the Stokes and anti-stokes thermometry, were also revealed.

Acknowledgments

The authors thank Prof. Filippo S. Boi for the helpful discussion. Project supported by the National Natural Science Foundation of China (Grant No. 12374013) and the Fundamental Research Funds for the Central Universities (Grant No. 2020SCUNL107).

References

[1] Jain S C, Willander M, Narayan J and Overstraeten R V 2000 *J. Appl. Phys.* **87** 965
[2] Figge S, Kröncke H, Hommel D and Epelbaum B M 2009 *Appl. Phys. Lett.* **94** 101915
[3] Amano H, Sawaki N, Akasaki I and Toyoda Y 1986 *Appl. Phys. Lett.* **48** 353
[4] Chang I F and Mitra S S 1971 *Adv. Phys.* **20** 359
[5] Klochikhin A A, Davydov V Y, Goncharuk I N, Smirnov A N, Nikolaev A E, Baidakova M V, Aderhold J, Graul J, Stemmer J and Semchinova O 2000 *Phys. Rev. B* **62** 2522
[6] Correia M R, Pereira S, Pereira E, Frandon J and Alves E 2003 *Appl. Phys. Lett.* **83** 4761
[7] Gebicki W, Strzeszewski J, Kamler G, Szyszko T and Podsiadło S 2000 *Appl. Phys. Lett.* **76** 3870
[8] Schubert M, Kasic A, Tiwald T E, Off J, Kuhn B and Scholz F 1999 *MRS Internet J. Nitride Semicond. Res.* **4** e11
[9] Pomeroy J W, Kuball M, Uren M J and Martin T 2008 *Phys. Status Solidi B* **245** 910
[10] Link A, Bitzer K, Limmer W, Sauer R, Kirchner C, Schwegler V, Kamp M, Ebling D G and Benz K W 1999 *J. Appl. Phys.* **86** 6256
[11] Pu X D, Chen J, Shen W Z, Ogawa H and Guo Q X 2005 *J. Appl. Phys.* **98** 033527
[12] Guo L L, Zhang Y H and Shen W Z 2006 *Appl. Phys. Lett.* **89** 161920
[13] Demangeot F, Groenen J, Frandon J, Renucci M A, Briot O, Clur S and Aulombard R L 1998 *Appl. Phys. Lett.* **72** 2674
[14] Wieser N, Ambacher O, Angerer H, Dimitrov R, Stutzmann M, Stritzker B and Lindner J K N 1999 *Phys. Status Solidi B* **216** 807
[15] Yu S, Kim K W, Bergman L, Dutta M, Stroscio M A and Zavada J M 1998 *Phys. Rev. B* **58** 15283
[16] Davydov V Yu, Goncharuk I N, Smirnov A N, Nikolaev A E, Lundin W V, Usikov A S, Klochikhin A A, Aderhold J, Graul J, Semchinova O and Harima H 2002 *Phys. Rev. B* **65** 125203
[17] Kosemura D, Sodan V and De Wolf I 2017 *J. Appl. Phys.* **121** 035702
[18] Liu Y, Yang X, Chen D, Lu H, Zhang R and Zheng Y 2015 *Adv. Condens. Matter Phys.* **2015** 1
[19] Chen D J, Shen B, Wu X L, Shen J C, Xu F J, Zhang K X, Zhang R, Jiang R L, Shi Y and Zheng Y D 2005 *Appl. Phys. A* **80** 1729
[20] Tao Y, Zhang L and Lei L 2022 *Phys. Rev. B* **105** 174102
[21] Liu J, Tao Y, Fan C, Wu B, Tang Q and Lei L 2022 *Chin. Phys. B* **31** 037801
[22] Zhao M, Wu B, Liu J and Lei L 2023 *Chin. Phys. B* **32** 090704
[23] Gorczyca I, Christensen N E, Peltzer Y Blancá E L and Rodriguez C O 1995 *Phys. Rev. B* **51** 11936
[24] Davydov V Yu, Kitaev Yu E, Goncharuk I N, Smirnov A N, Graul J, Semchinova O, Uffmann D, Smirnov M B, Mirgorodsky A P and Evarestov R A 1998 *Phys. Rev. B* **58** 12899
[25] Cantarero A, Cros A, Garro N, Gómez-Gómez M I, García A, De Lima M M, Daudin B, Rizzi A, Denker C and Malindretos J 2011 *Ann. Phys. (Berlin)* **523** 51
[26] Menéndez J and Cardona M 1984 *Phys. Rev. B* **29** 2051
[27] Li W S, Shen Z X, Feng Z C and Chua S J 2000 *J. Appl. Phys.* **87** 3332
[28] Wang D H, Xu T H and Song H Y *Acta Phys. Sin.* **65** 130702 (in Chinese)
[29] Cuscó R, Gil B, Cassabois G and Artús L 2016 *Phys. Rev. B* **94** 155435
[30] Peña-Alvarez M, Dalladay-Simpson P, Liu X D, Afonina V, Zhang H C, Howie R T and Gregoryanz E 2019 *J. Appl. Phys.* **125** 025901
[31] Goncharov A F, Crowhurst J C, Struzhkin V V and Hemley R J 2008 *Phys. Rev. Lett.* **101** 095502
[32] Santoro M, Lin J, Mao H and Hemley R J 2004 *J. Chem. Phys.* **121** 2780
[33] Kip B J and Meier R J 1990 *Appl. Spectro.* **44** 707
[34] Lin J F, Santoro M, Struzhkin V V, Mao H and Hemley R J 2004 *Rev. Sci. Instrum.* **75** 3302